Research Article

An Approach for Stability Analysis of Gas/Fluid-Filled Cylindrical Hole in Laminated Materials

Song Leng [ID]**, Li Hou** [ID]**, and Yang Duan**

School of Mechanical Engineering, Sichuan University, Chengdu, Sichuan 610065, China

Correspondence should be addressed to Song Leng; lengcool0505@163.com and Li Hou; houlaoshishiyanshi@163.com

An explicit analytical workflow for cylindrical hole stability analyses in general laminated materials that possess transversely isotropic (TI) anisotropy is presented. In this approach, the calculation of the distribution of the stresses around a cylindrical hole and the failure evaluation at the hole wall consider the effects of both material elasticity anisotropy and strength anisotropy caused by material laminated structures. Material strength anisotropy is assumed to be caused by the sliding of preexisting weakness planes oriented parallel to the isotropic plane of the material. The effect of anisotropy on strength is modeled by combining a shear failure criterion for the intact matrix and a weak plane failure criterion for the planes of weakness. We derive critical pressure solutions for the stability of the intact matrix around a hole filled with gas or fluid based on the Mohr–Coulomb failure criterion and Drucker–Prager failure criterion; either one of them can be combined with the weak plane failure criterion to give the solution for hole wall shear failure pressure. The solution for hole wall fracture initiation pressure is derived based on the tensile failure criterion. This approach can be applied to holes of arbitrary orientation in general laminated materials.

1. Introduction

Traditional mechanical parts are mostly made of isotropic materials. Nowadays, the innovation and advancement in material production and processing methods promote the development of more sophisticated mechanical parts that can exhibit anisotropy, such as laminated composite parts, functionally graded material parts, and additive manufacturing parts. Some originally isotropic metal parts can also become anisotropic after a long period of usage due to metal fatigue or degradation. The abovementioned various types of parts often exhibit laminated features. Their elasticity can be effectively modeled as transverse isotropy, meaning that the mechanical properties are symmetric about an axis that is normal to the laminated structures. Either intrinsic or usage-induced anisotropy can make the mechanical response of a material sensitive to loading direction; thus, it is important to understand the mechanical stability of anisotropic parts before they can be used in industry applications.

The mechanical concepts, theories, calculation approaches, or experimental methods established based on uniformly isotropic materials may not be directly applied for analyzing laminated materials. The inherent nonuniformity of their mechanical performance can make the mechanical analyses complicated. There are a number of different approaches developed for studying this type of problems. Silling and Askari [1, 2] introduced the dynamics theory for modeling damage and fracture in isotropic materials [1–4] and composite materials. This approach can avoid the mathematical difficulty associated with material discontinuities by adopting an integral form of formulation in stress analysis. Chow et al. [5] presented a method of nonlinear damage analysis for anisotropic materials based on the concepts of damage surface and damage potential, and the new method was validated by its application to thin composite laminates. Sharma [6] studied the stress concentration around cutouts in an infinite layered composite plate subjected to arbitrary biaxial loading at infinity by using Muskhelisvili's complex variable method to obtain the

general stress functions, from which the stress distribution can be determined. Although the complex variable method is useful in solving various elastic problems, it must be reworked when it is applied to problems with different model configurations. Zaoui et al. [7] introduced the elastic basis parameters into a Hamiltonian formulation about motion and then derived the closed-form fundamental solution of the Pastenak mathematical model based on eigenvalue analysis. Mantari et al. [8] established a new high-order shear deformation theory for the static analysis of laminated composites and sandwich plates. The cylindrical hole structure is one of the most commonly used functional structures and process structures for various types of mechanical parts. However, there is no convenient approach for determining the mechanical safety of a laminated material with holes.

Traditional numerical modeling methods, such as finite element method (FEM) and boundary element method (BEM), are commonly used in mechanical analysis of laminates. But the computational cost of three-dimensional numerical simulations can be very high when a model contains finely laminated structures. Various gradient finite element methods [9–12] have been proposed to resolve the computational efficiency issue, but these methods have their limitations and can only be applied to solve certain problems. For example, Santare et al. [9, 12] benchmarked the result obtained from the gradient finite element method against the exact solution for a one-dimensional wave propagation problem and pointed out that the numerical error of finite element modeling is significant. The mechanical and mathematical modeling of laminates is still an active area of research so far.

Horgan and Chan [13] studied the stress response of a pressurized hollow cylinder made of a functionally linearly elastic isotropic material with the Young's modulus varying radially. Ying and Wang [14] proposed an analytical stress solution for a rotating multi-iron composite hollow cylinder made of radially polarized piezoelectric materials. Durodola and Attia [15] studied the deformation and stress of a functionally graded turntable and compared the modeling results obtained from a finite element method and a direct numerical integration method. Zhu et al. [16] numerically investigated the working condition of a composite sandwich cylindrical shell under hydrostatic pressure and predicted the critical failure pressure based on finite element modeling. In summary, numerical modeling of the stress distribution around a hole in a complex material is time consuming and the postanalysis for mechanical stability study is also not trivial. Considering the high complexity of model building and large computational cost of numerical modeling, practitioners would desire a fast and easy-to-use tool for stress analysis and stability evaluation for industry applications.

In this paper, we propose an analytical procedure for calculating the stresses around a cylindrical hole in general laminates and provide explicit solutions for evaluating the hole stability based on the Mohr–Coulomb failure criterion, Drucker–Prager failure criterion, weak plane failure criterion, and tensile failure criterion. The influence of the laminate internal discontinuities on mechanical stability is accounted for by incorporating the weak plane failure criterion into failure evaluation. The first two criteria (i.e., Mohr–Coulomb and Drucker–Prager) are used to model the failure of the intact matrix, and either one of them can be combined with the weak plane failure criterion to give the solution for hole wall shear failure pressure. The tensile failure criterion is used to find the fracture initiation pressure at the hole wall. These failure criteria together can determine the safe region of the hole working pressure for given loading conditions on a part.

2. Methodology

Three reference coordinate systems are used in the analysis. All input parameters, such as material stiffness matrix and boundary stress tensor, are assumed to be defined in a global coordinate system (GCS), XYZ, which should align with the geometry of the material. The second coordinate system is the cylindrical hole coordinate system (HCS), in which the z-axis points downward along the hole axis and the y-axis is parallel to the isotropic plane of the material. The last coordinate system is the hole cylindrical coordinate system (CCS) that is transformed from HCS.

In this section, we will first give a brief review of the method for calculating the distribution of hole stresses in general TI media and then derive the analytical solutions for critical hole gas/fluid pressure for several commonly used failure models.

2.1. Analytical Solution for Stress Distribution around a Circular Hole in an Arbitrary TI Material. Fang [17] presented the explicit analytical solution for stress distribution around a circular hole in an arbitrary transversely isotropic medium subjected to boundary stresses and hole internal fluid pressure. In his derivation, a hole is assumed to be infinite and homogeneous in the axial direction so that the problem can be simplified based on the generalized plain strain assumption. Hole wall is assumed to be impervious. The material surrounding the hole is assumed to possess transversely isotropy, but the elastic symmetry plane is not necessary to be parallel/normal to the hole axis, so the stiffness matrix of the material may have up to 21 nonzero components in GCS, although it only contains five independent components. Moreover, the boundary stresses may have six nonzero components because the hole and boundary principal stress directions in practices may not coincide. The constitutive relation can be expressed as

$$\sigma = \mathbf{C}^{(g)} \cdot \varepsilon, \tag{1}$$

where $\sigma = [\sigma_{xx}, \sigma_{yy}, \sigma_{zz}, \sigma_{yz}, \sigma_{xz}, \sigma_{xy}]^T$ and $\varepsilon = [\varepsilon_{xx}, \varepsilon_{yy}, \varepsilon_{zz}, 2\varepsilon_{yz}, 2\varepsilon_{xz}, 2\varepsilon_{xy}]^T$ are, respectively, the stress and strain vectors and the stiffness matrix $\mathbf{C}^{(g)}$ that is defined in GCS has the following general form:

$$\mathbf{C}^{(g)} = \begin{bmatrix} C_{11}^{(g)} & C_{12}^{(g)} & C_{13}^{(g)} & C_{14}^{(g)} & C_{15}^{(g)} & C_{16}^{(g)} \\ C_{12}^{(g)} & C_{22}^{(g)} & C_{23}^{(g)} & C_{24}^{(g)} & C_{25}^{(g)} & C_{26}^{(g)} \\ C_{13}^{(g)} & C_{23}^{(g)} & C_{33}^{(g)} & C_{34}^{(g)} & C_{35}^{(g)} & C_{36}^{(g)} \\ C_{14}^{(g)} & C_{24}^{(g)} & C_{34}^{(g)} & C_{44}^{(g)} & C_{45}^{(g)} & C_{46}^{(g)} \\ C_{15}^{(g)} & C_{25}^{(g)} & C_{35}^{(g)} & C_{45}^{(g)} & C_{55}^{(g)} & C_{56}^{(g)} \\ C_{16}^{(g)} & C_{26}^{(g)} & C_{36}^{(g)} & C_{46}^{(g)} & C_{56}^{(g)} & C_{66}^{(g)} \end{bmatrix}. \tag{2}$$

A cylindrical hole with radius R is subjected to the hole internal gas/fluid pressure P_w and the boundary stress condition that is denoted as

$$\boldsymbol{\sigma}^{(g)} = \begin{bmatrix} \sigma_{xx}^{(g)} & \sigma_{xy}^{(g)} & \sigma_{xz}^{(g)} \\ \sigma_{xy}^{(g)} & \sigma_{yy}^{(g)} & \sigma_{yz}^{(g)} \\ \sigma_{xz}^{(g)} & \sigma_{yz}^{(g)} & \sigma_{zz}^{(g)} \end{bmatrix}. \tag{3}$$

One needs to first transform $\mathbf{C}^{(g)}$ and $\boldsymbol{\sigma}^{(g)}$ from GCS to HCS and then solve for the hole stress solution in HCS. Appendix gives an overview of the derivation process. In HCS, the stress solution can be written as

$$\boldsymbol{\sigma} = \boldsymbol{\sigma}^{(0)} + \boldsymbol{\sigma}^{(i)} + \mathbf{q} \cdot P_w, \tag{4}$$

with

$$\boldsymbol{\sigma}^{(0)} = \mathbf{E} \cdot \boldsymbol{\sigma}^{(g)} \cdot \mathbf{E}^T = \begin{bmatrix} \sigma_{xx}^{(0)} & \sigma_{xy}^{(0)} & \sigma_{xz}^{(0)} \\ \sigma_{xy}^{(0)} & \sigma_{yy}^{(0)} & \sigma_{yz}^{(0)} \\ \sigma_{xz}^{(0)} & \sigma_{yz}^{(0)} & \sigma_{zz}^{(0)} \end{bmatrix},$$

$$\boldsymbol{\sigma}^{(i)} = \boldsymbol{\sigma}^{(i)}\left(\mathbf{C}^{(g)}, \boldsymbol{\sigma}^{(g)}\right) = \begin{bmatrix} \sigma_{xx}^{(i)} & \sigma_{xy}^{(i)} & \sigma_{xz}^{(i)} \\ \sigma_{xy}^{(i)} & \sigma_{yy}^{(i)} & \sigma_{yz}^{(i)} \\ \sigma_{xz}^{(i)} & \sigma_{yz}^{(i)} & \sigma_{zz}^{(i)} \end{bmatrix}, \tag{5}$$

$$\mathbf{q} = \mathbf{q}\left(\mathbf{C}^{(g)}\right) = \begin{bmatrix} q_1 & q_3 & q_4 \\ q_3 & q_2 & q_5 \\ q_4 & q_5 & q_6 \end{bmatrix},$$

where the first term in equation (4), $\boldsymbol{\sigma}^{(0)}$, is the boundary stress tensor in HCS, the second term, $\boldsymbol{\sigma}^{(i)}$, which is a function of $\boldsymbol{\sigma}^{(g)}$ and $\mathbf{C}^{(g)}$, is the stress alteration induced by boundary stresses, the matrix $\mathbf{q}$ that depends only on material property characterizes the effect of the hole gas/fluid pressure on individual stress components, $\mathbf{E}$ is the coordinate transformation matrix that is defined by equation (A.7). Expressions for the components in $\boldsymbol{\sigma}^{(i)}$ and $\mathbf{q}$ are given by equations (A.40)–(A.76).

Fang [17] demonstrated that the explicit analytical expression for equation (4) can be obtained and used for hole stress calculation in arbitrary transversely isotropic media regardless of the hole orientation relative to the material elasticity symmetry axis. Moreover, this solution is valid for degenerate isotropic cases.

2.2. Solutions for Critical Hole Fluid Pressure.

In the previous section, the explicit analytical solution for stress distribution around a cylindrical hole in a general TI medium for given boundary stress conditions and hole internal gas/fluid pressure is presented. With adopted failure criteria, this hole stress solution can be used for failure evaluation of the hole wall. Explicit solutions of critical hole pressure for both shear and tensile failure are derived in this section. For shear failure, the Mohr–Coulomb and Drucker–Prager criteria are discussed separately and the weak plane approach is used to model the effect of strength anisotropy that is induced by material internal discontinuities.

The stress tensor is transformed from HCS to CCS in order to perform the failure analysis:

$$\widetilde{\sigma} = \mathbf{T} \cdot \boldsymbol{\sigma} \cdot \mathbf{T}^T = \widetilde{\sigma}^{(f)} + \widetilde{q} \cdot P_w, \tag{6}$$

with

$$\widetilde{\sigma}^{(f)} = \mathbf{T} \cdot \left[\boldsymbol{\sigma}^{(0)} + \boldsymbol{\sigma}^{(i)}\right] \cdot \mathbf{T}^T, \tag{7}$$

$$\widetilde{q} = \mathbf{T} \cdot \mathbf{q} \cdot \mathbf{T}^T, \tag{8}$$

$$\mathbf{T} = \begin{bmatrix} \cos\theta & \sin\theta & 0 \\ -\sin\theta & \cos\theta & 0 \\ 0 & 0 & 1 \end{bmatrix}. \tag{9}$$

Since the initiation of elastic failure is expected to occur at the hole wall, the calculation of critical hole gas/fluid pressure concerns the stresses at the hole wall $r = R$ only. The components of the stress tensor $\widetilde{\sigma}$ (equation (6)) at $r = R$ are expressed as

$$\begin{aligned} \widetilde{\sigma}_{\theta\theta} &= \widetilde{\sigma}_{\theta\theta}^{(f)} + \widetilde{q}_{\theta\theta} P_w, \\ \widetilde{\sigma}_{zz} &= \widetilde{\sigma}_{zz}^{(f)} + \widetilde{q}_{zz} P_w, \\ \widetilde{\sigma}_{\theta z} &= \widetilde{\sigma}_{\theta z}^{(f)} + \widetilde{q}_{\theta z} P_w, \\ \widetilde{\sigma}_{rr} &= P_w, \\ \widetilde{\sigma}_{r\theta} &= \widetilde{\sigma}_{rz} = 0. \end{aligned} \tag{10}$$

The corresponding three principal stresses can be expressed as

$$\sigma_1(\theta) = \frac{\widetilde{\sigma}_{\theta\theta} + \widetilde{\sigma}_{zz}}{2} + \sqrt{\left(\frac{\widetilde{\sigma}_{\theta\theta} - \widetilde{\sigma}_{zz}}{2}\right)^2 + \widetilde{\sigma}_{\theta z}^2}, \tag{11}$$

$$\sigma_2(\theta) = \frac{\widetilde{\sigma}_{\theta\theta} + \widetilde{\sigma}_{zz}}{2} - \sqrt{\left(\frac{\widetilde{\sigma}_{\theta\theta} - \widetilde{\sigma}_{zz}}{2}\right)^2 + \widetilde{\sigma}_{\theta z}^2}, \tag{12}$$

$$\sigma_3 = \widetilde{\sigma}_{rr}. \tag{13}$$

Note that the subscripts $_{1,2,3}$ in equations (11)–(13) do not represent their relative magnitude. σ_1 and σ_2 vary with the hole wall azimuth θ, while σ_3 is independent of θ. By inserting the expressions for $\widetilde{\sigma}_{ij}$ into equations (11)–(13), one can obtain

$$\sigma_1(\theta) = eP_w + f + \sqrt{gP_w^2 + hP_w + s}, \tag{14}$$

$$\sigma_2(\theta) = eP_w + f - \sqrt{gP_w^2 + hP_w + s}, \tag{15}$$

$$\sigma_3 = P_w. \tag{16}$$

The coefficients e, f, g, h, and s are expressed as

$$
\begin{aligned}
e &= \frac{1}{2}\left(\tilde{q}_{\theta\theta} + \tilde{q}_{zz}\right), \\
f &= \frac{1}{2}\left(\tilde{\sigma}_{\theta\theta}^{(f)} + \tilde{\sigma}_{zz}^{(f)}\right), \\
g &= \left(\frac{\tilde{q}_{\theta\theta} - \tilde{q}_{zz}}{2}\right)^2 + \tilde{q}_{\theta z}^2, \\
h &= \frac{1}{2}\left(\tilde{q}_{\theta\theta} - \tilde{q}_{zz}\right)\left(\tilde{\sigma}_{\theta\theta}^{(f)} - \tilde{\sigma}_{zz}^{(f)}\right) + 2\tilde{q}_{\theta z}\tilde{\sigma}_{\theta z}^{(f)}, \\
s &= \left(\frac{\tilde{\sigma}_{\theta\theta}^{(f)} - \tilde{\sigma}_{zz}^{(f)}}{2}\right)^2 + \left(\tilde{\sigma}_{\theta z}^{(f)}\right)^2.
\end{aligned}
\tag{17}
$$

2.3. Mohr–Coulomb Shear Failure.

The Mohr–Coulomb failure criterion can be expressed as

$$f_{\mathrm{MC}} = \sigma_{\max} - \left(C_1 + C_2\sigma_{\min}\right), \{<0: \text{stable}; \geq 0: \text{unstable}\}, \tag{18}$$

where $\sigma_{\min}$ and $\sigma_{\max}$ are, respectively, the minimum and maximum principle stresses, C_1 and C_2 are the material coefficients that can be related to the cohesion, S_0, and friction angle, φ, of a material:

$$
\begin{aligned}
C_1 &= 2S_0\frac{\cos\varphi}{1 - \sin\varphi}, \\
C_2 &= \frac{1 + \sin\varphi}{1 - \sin\varphi}.
\end{aligned}
\tag{19}
$$

Depending on the relative magnitude of σ_1, σ_2, and σ_3, there are three possible cases: (1) $\sigma_{\min} = \sigma_2$, $\sigma_{\max} = \sigma_1$; (2) $\sigma_{\min} = \sigma_3$, $\sigma_{\max} = \sigma_1$; and (3) $\sigma_{\min} = \sigma_2$, $\sigma_{\max} = \sigma_3$.

Case 1. $\sigma_{\min} = \sigma_2$ and $\sigma_{\max} = \sigma_1$

Insert equations (14) and (15) into (18) and make the expression equal to zero, which represents the failure surface; the failure criterion can be rewritten as

$$(1 + C_2)\sqrt{gP_w^2 + hP_w + s} = e(C_2 - 1)P_w + (C_2 - 1)f + C_1. \tag{20}$$

The stable condition requires the term on the left side of equation (20) to be smaller than the other term on the right side. By taking the square of both sides of equation (20), one can obtain the following quadratic equation:

$$E'P_w^2 + F'P_w + G' = 0, \tag{21}$$

with

$$
\begin{aligned}
E' &= (1 + C_2)^2 g - e^2(C_2 - 1)^2, \\
F' &= (1 + C_2)^2 h - 2e(C_2 - 1)\left[C_1 + (C_2 - 1)f\right], \\
G' &= (1 + C_2)^2 s - \left[C_1 + (C_2 - 1)f\right]^2.
\end{aligned}
\tag{22}
$$

The roots to equation (21) are not necessary to be the solutions to equation (20), because the square operation may introduce a fictitious root. Equation (21) may have one or two roots depending on the value of the quadratic coefficient E'. Figure 1 schematically illustrates the relationship between the expressions on the left (solid curve) and right (dashed line) sides of equation (20). The slope of the linear function on the right side of equation (20) is always negative because $e < 0$ and $C_2 > 1$. The gray region, in which the solid curve is smaller than the dashed line, represents the range of stable P_w. When $E' > 0$, the stable hole pressure P_w is bounded within a finite range, whose upper and lower bounds are the two roots of equation (21). When $E' = 0$, equation (21) reduces to a linear equation whose root defines the upper bound of safe P_w. When $E' < 0$, equation (20) has only one root, which is equal to the smaller root of equation (21). The larger root of equation (21) is a fictitious root that is introduced by the square operation. It corresponds to the intersection of the conjugate of the linear function on the right side of equation (20) and the other function on the left side. The lower and upper bounds of the safe P_w can be written in the following concise form:

$$
P_l'(\theta) = \begin{cases} \dfrac{-F' - \sqrt{\Delta'}}{2E'}, & \Delta' > 0 \quad \text{and} \quad E' > 0, \\[3mm] -\infty, & E' \leq 0, \end{cases}
$$
$$
P_u'(\theta) = \begin{cases} \dfrac{-F' + \sqrt{\Delta'}}{2E'}, & \Delta' > 0 \quad \text{and} \quad E' \neq 0, \\[3mm] -\dfrac{G}{F'}, & E' = 0, \end{cases}
\tag{23}
$$

with

$$\Delta' = F'^2 - 4E'G'. \tag{24}$$

P_l' and P_u' are functions of hole azimuth θ. The maximum P_l' over all azimuths is the collapse pressure of hole wall, below which shear failure will occur. The minimum P_u' over all azimuths is the allowed maximum hole pressure, above which passive shear failure will occur. The interval between the upper and lower bounds is the safe pressure region for given boundary stress conditions and material properties.

Case 2. $\sigma_{\min} = \sigma_3$ and $\sigma_{\max} = \sigma_1$

Insert equations (14) and (16) into equation (18), the failure criterion can be rewritten as
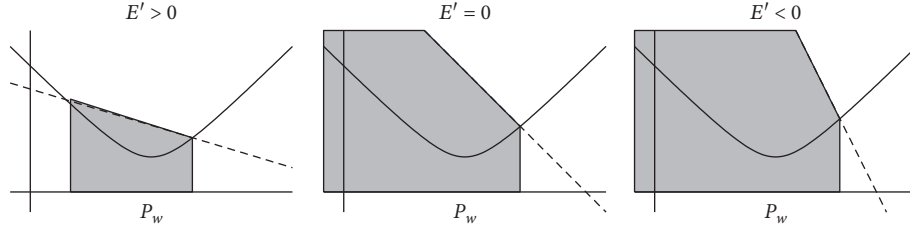
FIGURE 1: Schematic illustrates the range of stable hole pressure P_w for the Mohr–Coulomb model when $\sigma_{\min} = \sigma_2$ and $\sigma_{\max} = \sigma_1$. The black curve and dashed line, respectively, represent the expressions on the left and right sides of equation (20). The gray region is the stable hole pressure range in which the values of the dashed line are larger than those of the solid curve. The parameter E', which is defined by equation (21), represents the relative magnitude of the slopes of the dashed line and the asymptote of the solid curve at infinity.

$$\sqrt{gP_w^2 + hP_w + s} = (C_2 - e)P_w + C_1 - f. \qquad (25)$$

Similar to the previous discussion, there are three possible situations depending on the value of the quadratic coefficient of the quadratic equation obtained by taking the square of both sides of equation (25):

$$E'' P_w^2 + F'' P_w + G'' = 0, \qquad (26)$$

with

$$
\begin{aligned}
E'' &= g - (C_2 - e)^2, \\
F'' &= h - 2(C_2 - e)(C_1 - f), \\
G'' &= s - (C_1 - f)^2.
\end{aligned}
\qquad (27)
$$

Figure 2 shows the relationship between the functions on the left (solid curve) and right (dashed line) sides of equation (25). Contrary to the previous case, the slope of the linear function on the right side of equation (25) is always positive because $C_2 > 0$ and $e < 0$. When $E'' > 0$, the two roots of equation (26) are also the roots for equation (25). When $E'' \leq 0$, as shown in Figure 2, the solid curve and dashed line have only one intersection, and thus, equation (25) has one root. The lower and upper bounds of the safe hole pressure can be written in the following form:

$$
P_l''(\theta) =
\begin{cases}
\dfrac{-F'' - \sqrt{\Delta''}}{2E''}, & \Delta'' > 0 \quad \text{and} \quad E'' \neq 0, \\[3mm]
-\dfrac{G''}{F''}, & E'' = 0,
\end{cases}
\qquad (28)
$$

$$
P_u''(\theta) =
\begin{cases}
\dfrac{-F'' + \sqrt{\Delta''}}{2E''}, & \Delta'' > 0 \quad \text{and} \quad E'' > 0, \\[3mm]
+\infty, & E'' \leq 0,
\end{cases}
\qquad (29)
$$

with

$$\Delta'' = F''^2 - 4E''G''. \qquad (30)$$

Case 3. $\sigma_{\min} = \sigma_2$ and $\sigma_{\max} = \sigma_3$

Inserting equations (15) and (16) into equation (18), the failure criterion can be rewritten as

$$C_2 \sqrt{gP_w^2 + hP_w + s} = (eC_2 - 1)P_w + C_1 + fC_2. \qquad (31)$$

Because the slope of the linear function on the right side of equation (31) is negative, the derivation of the roots for equation (31) is similar to that for Case 1. The quadratic equation obtained through square operation is given as

$$E''' P_w^2 + F''' P_w + G''' = 0, \qquad (32)$$

with

$$
\begin{aligned}
E''' &= gC_2^2 - (eC_2 - 1)^2, \\
F''' &= hC_2^2 - 2(eC_2 - 1)(C_1 + fC_2), \\
G''' &= sC_2^2 - (C_1 + fC_2)^2.
\end{aligned}
\qquad (33)
$$

Similar to the previous procedure, the lower and upper bounds of the safe hole wall pressure can be obtained as

$$
P_l''(\theta) =
\begin{cases}
\dfrac{-F''' - \sqrt{\Delta'''}}{2E'''}, & \Delta''' > 0 \quad \text{and} \quad E''' > 0, \\[3mm]
-\infty, & E''' \leq 0,
\end{cases}
\qquad (34)
$$

$$
P_u''(\theta) =
\begin{cases}
\dfrac{-F''' + \sqrt{\Delta'''}}{2E'''}, & \Delta''' > 0 \quad \text{and} \quad E'''0, \\[3mm]
-\dfrac{G'''}{F'''}, & E''' = 0,
\end{cases}
\qquad (35)
$$

with

$$\Delta''' = F'''^2 - 4E'''G'''. \qquad (36)$$

The stable region of hole pressure that fulfills the failure criterion of equation (18) can be obtained by consolidating the solutions for the above three cases. At a given hole azimuth θ, the lower and upper bounds of the stable hole pressure range, in which the hole wall will not fail along that particular azimuth, are, respectively, given as
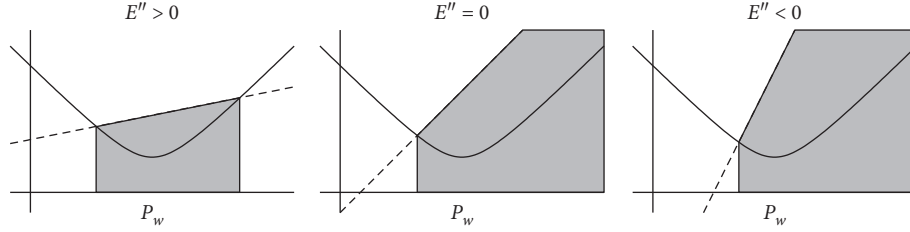
Figure 2: Schematic illustrates the range of stable hole pressure P_w for the Mohr–Coulomb model when $\sigma_{\min} = \sigma_3$ and $\sigma_{\max} = \sigma_1$. The black curve and dashed line, respectively, represent the expressions on the left and right sides of equation (25). The gray region is the stable hole pressure range in which the values of the dashed line are larger than those of the solid curve. The parameter E'', which is defined by equation (26), represents the relative magnitude of the slopes of the dashed line and the asymptote of the solid curve at infinity.

$$P_l^{(MC)}(\theta) = \max\left(P_l'(\theta), P_l''(\theta), P_l'''(\theta)\right),$$
$$P_u^{(MC)}(\theta) = \min\left(P_u'(\theta), P_u''(\theta), P_u'''(\theta)\right). \tag{37}$$

By definition, the hole critical pressure is the failure initiation pressure. The hole collapse pressure is the maximum of $P_l^{(MC)}$ over all azimuths. Similarly, the passive shear failure pressure is the minimum of $P_u^{(MC)}$ over all azimuths. Thus, the hole collapse pressure and passive shear failure pressure for the Mohr–Coulomb failure criterion can be, respectively, expressed as

$$P_L^{(MC)} = \max_{\theta \in [0, 2\pi]}\left(P_l^{(MC)}(\theta)\right), \tag{38}$$

$$P_U^{(MC)} = \min_{\theta \in [0, 2\pi]}\left(P_u^{(MC)}(\theta)\right). \tag{39}$$

Equations (38) and (39) can be evaluated by simply using a grid search approach to search over the entire hole azimuth. The computational cost for finding the minimum/maximum values is negligible, as $P_l^{(MC)}(\theta)$ and $P_u^{(MC)}(\theta)$ are given in explicit forms.

2.4. Drucker–Prager Shear Failure.
Drucker–Prager shear failure criterion is written as

$$f_{DP} = \sqrt{J_2} - (A + BI_1), \{<0: \text{stable}; \geq 0: \text{unstable}\}, \tag{40}$$

with

$$I_1 = \sigma_1 + \sigma_2 + \sigma_3,$$
$$J_2 = \frac{1}{6}\left[(\sigma_1 - \sigma_2)^2 + (\sigma_2 - \sigma_3)^2 + (\sigma_1 - \sigma_3)^2\right],$$
$$A = \frac{6S_0\cos\varphi}{\sqrt{3}(3 - \sin\varphi)}, \tag{41}$$
$$B = \frac{2\sin\varphi}{\sqrt{3}(3 - \sin\varphi)},$$

where I_1 and J_2 are the stress invariants and A and B are the parameters associated with cohesion, S_0, and friction angle, φ.

Insert equations (14)–(16) into equation (40) and make the expression equal to zero; after some algebraic manipulations, equation (40) becomes

$$\sqrt{\left[g + \frac{1}{3}(e - 1)^2\right]P_w^2 + \left[h + \frac{2}{3}f(e - 1)\right]P_w + s + \frac{1}{3}f^2}$$
$$= B(2e + 1)P_w + A + 2Bf. \tag{42}$$

Equation (40) must have two roots so that the range of stable hole pressure is bounded. Otherwise, the solution is physically unreal. Taking the square of both sides of equation (40) and rearranging the terms, the following quadratic equation can be obtained:

$$EP_w^2 + FP_w + G = 0, \tag{43}$$

with

$$E = g + \frac{1}{3}(e - 1)^2 - B^2(2e + 1)^2,$$

$$F = h + \frac{2}{3}f(e - 1) - 2B(2e + 1)(A + 2Bf), \tag{44}$$

$$G = s + \frac{1}{3}f^2 - (A + 2Bf)^2.$$

When $F^2 > 4EG$, equation (43) has two roots that correspond to the lower and upper bounds of the safe hole pressure:

$$P_l^{(DP)}(\theta) = \frac{-F - \sqrt{F^2 - 4EG}}{2E},$$
$$P_u^{(DP)}(\theta) = \frac{-F + \sqrt{F^2 - 4EG}}{2E}. \tag{45}$$

The hole collapse pressure and passive shear failure pressure for the Drucker–Prager failure criterion can be, respectively, expressed as

$$P_L^{(DP)} = \max_{\theta \in [0,2\pi]} \left(P_l^{(DP)}(\theta) \right), \tag{46}$$

$$P_U^{(DP)} = \min_{\theta \in [0,2\pi]} \left(P_u^{(DP)}(\theta) \right). \tag{47}$$

2.5. Weak Plane Model.

The previous failure models are only applicable to intact matrix. In order to model the anisotropic strength behavior of laminated materials, the weak plane approach is used to model the shear failure along the planes of weakness. The failure criterion for a plane of weakness is

$$f_{WP} = |\tau| - (\mu_w \sigma_n + S_w), \quad \{<0: \text{stable}; \geq 0: \text{unstable}\}, \tag{48}$$

where τ and σ_n are, respectively, the shear and normal stresses acting on the plane of weakness, S_w is the intrinsic shear strength in the plane of weakness, and μ_w is the sliding friction coefficient of the weak plane.

It is assumed that the plane of weakness coincides with the isotropic plane of a medium. Since the y-axis is parallel to the isotropic plane (i.e., the weak plane) in HCS, the normal to the weak plane lies in the x-z plane, as shown in Figure 3. If the stiffness matrix is rotated about the y-axis in HCS by an angle θ_w, which is the angle between the weak plane normal and the x-axis, the x-axis becomes normal to the isotropic plane after the rotation, resulting in the elimination of the elastic constants C_{15}, C_{25}, C_{35}, and C_{46}. Comparing the stiffness matrix before and after the rotation, one can obtain the following relationships:

$$C_{25} \cos 2\theta_w + \frac{1}{2}(C_{23} - C_{12})\sin 2\theta_w = 0,$$
$$C_{46} \cos 2\theta_w + \frac{1}{2}(C_{44} - C_{66})\sin 2\theta_w = 0. \tag{49}$$

Then, θ_w can be directly determined from the elastic constants:

$$\theta_w = \begin{cases} \dfrac{1}{2}\cot^{-1}\left(\dfrac{C_{12} - C_{23}}{2C_{25}}\right), & \text{if}\, C_{25} \neq 0, \\[3mm] \dfrac{1}{2}\cot^{-1}\left(\dfrac{C_{66} - C_{44}}{2C_{46}}\right), & \text{if}\, C_{25} = 0 \quad \text{and} \quad C_{46} \neq 0. \end{cases} \tag{50}$$

There are two possibilities that would lead to $C_{25} = C_{46} = 0$: (1) $\theta_w = 0°$ or $90°$; this indicates that the TI symmetric axis coincides with one of the coordinate axes, resulting in $C_{15} = C_{25} = C_{35} = C_{46} = 0$. (2) $C_{23} = C_{12}$ and $C_{44} = C_{66}$; this implies that the y-axis is normal to the

isotropic plane of the formation when the formation is anisotropic, which is not possible as it contradicts the definition of the HCS. If θ_w is a known parameter, then there is no need to calculate it using equation (50).

To calculate the stresses acting on the weak plane, rotate the stress tensor at the hole wall about the y-axis in HCS by an angle θ_w:

$$\widetilde{\widetilde{\sigma}} = \mathbf{T}_w \cdot \boldsymbol{\sigma} \cdot T_w^T = \widehat{\sigma} + \widehat{q} \cdot P_w, \tag{51}$$

with

$$\widehat{\sigma} = \mathbf{T}_w \cdot \left[\boldsymbol{\sigma}^{(0)} + \boldsymbol{\sigma}^{(i)} \right] \cdot \mathbf{T}_w^T, \tag{52}$$

$$\widehat{q} = \mathbf{T}_w \cdot \mathbf{q} \cdot \mathbf{T}_w^T, \tag{53}$$

$$\mathbf{T}_w = \begin{bmatrix} \cos\theta_w & 0 & \sin\theta_w \\ 0 & 1 & 0 \\ -\sin\theta_w & 0 & \cos\theta_w \end{bmatrix}. \tag{54}$$

After the rotation, $\widetilde{\widetilde{\sigma}}_{xx}$ is normal to the weak plane, while $\widetilde{\widetilde{\sigma}}_{yy}$ and $\widetilde{\widetilde{\sigma}}_{zz}$ are parallel to it. The stress acting on the weak plane is given as

$$\overrightarrow{T}_n = \widetilde{\widetilde{\sigma}} \cdot \overrightarrow{n} = \begin{bmatrix} \widehat{\sigma}_{xx} + \widehat{q}_{xx} P_w \\ \widehat{\sigma}_{xy} + \widehat{q}_{xy} P_w \\ \widehat{\sigma}_{xz} + \widehat{q}_{xz} P_w \end{bmatrix}, \tag{55}$$

where the normal vector $\overrightarrow{\mathbf{n}} = [1, 0, 0]^T$.

The normal stress is

$$\sigma_n = [\overrightarrow{n}]^T \cdot \overrightarrow{T}_n = \widehat{\sigma}_{xx} + \widehat{q}_{xx} P_w. \tag{56}$$

The magnitude of shear stress is

$$|\tau| = \sqrt{\left| \overrightarrow{T}_n \right|^2 - \sigma_n^2}$$
$$= \sqrt{P_w^2 \left(\widehat{q}_{xy}^2 + \widehat{q}_{xz}^2 \right) + 2P_w \left(\widehat{\sigma}_{xy}\widehat{q}_{xy} + \widehat{\sigma}_{xz}\widehat{q}_{xz} \right) + \widehat{\sigma}_{xy}^2 + \widehat{\sigma}_{xz}^2}. \tag{57}$$

Inserting equations (56) and (57) into equation (48), one can obtain

$$\sqrt{P_w^2 \left(\widehat{q}_{xy}^2 + \widehat{q}_{xz}^2 \right) + 2P_w \left(\widehat{\sigma}_{xy}\widehat{q}_{xy} + \widehat{\sigma}_{xz}\widehat{q}_{xz} \right) + \widehat{\sigma}_{xy}^2 + \widehat{\sigma}_{xz}^2}$$
$$= \widehat{q}_{xx}\mu_w P_w + \mu_w \widehat{\sigma}_{xx} + S_w. \tag{58}$$

Take the square of both sides of equation (58); one can obtain the following quadratic equation:
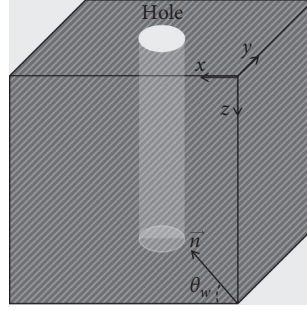
$$EP_w^2 + FP_w + G = 0, \tag{59}$$

with

FIGURE 3: Schematic illustrates the hole coordinate system (HCS), in which the z-axis is along the hole axis direction and the y-axis is parallel to the material isotropic plane that is represented by the gray lines. $\vec{n}$ is the normal to the material isotropic plane (i.e., the material symmetry axis direction). θ_w is the angle between $\vec{n}$ and the x-axis.

$$
\begin{aligned}
E &= \hat{q}_{xy}^2 + \hat{q}_{xz}^2 - \mu_w^2 \hat{q}_{xx}^2, \\
F &= 2\left(\hat{\sigma}_{xy}\hat{q}_{xy} + \hat{\sigma}_{xz}\hat{q}_{xz}\right) - 2\mu_w\hat{q}_{xx}\left(\mu_w\hat{\sigma}_{xx} + S_w\right), \\
G &= \hat{\sigma}_{xy}^2 + \hat{\sigma}_{xz}^2 - \left(\mu_w\hat{\sigma}_{xx} + S_w\right)^2.
\end{aligned} \tag{60}
$$

Similar to the Mohr–Coulomb model, the solution for equation (58) depends on the sign of the slope of the linear term on the right side and the value of E in equation (59). Following the previous analysis procedure, one can obtain the lower and upper bounds for the safe hole pressure as

$$
P_l^{(WP)}(\theta) = \begin{cases} \dfrac{-F - \sqrt{F^2 - 4EG}}{2E}, & E \neq 0 \quad \text{and} \quad F^2 > 4EG, \\[3mm] -\dfrac{G}{F}, & E = 0, \end{cases}
$$

$$
P_u^{(WP)}(\theta) = \begin{cases} \dfrac{-F + \sqrt{F^2 - 4EG}}{2E}, & E > 0 \quad \text{and} \quad F^2 > 4EG, \\[3mm] +\infty, & E \leq 0, \end{cases} \tag{61}
$$

for $\hat{q}_{xx} \geq 0$, and

$$
P_l^{(WP)}(\theta) = \begin{cases} \dfrac{-F - \sqrt{F^2 - 4EG}}{2E}, & E > 0 \quad \text{and} \quad F^2 > 4EG, \\[3mm] -\infty, & E \leq 0, \end{cases}
$$

$$
P_u^{(WP)}(\theta) = \begin{cases} \dfrac{-F + \sqrt{F^2 - 4EG}}{2E}, & E \neq 0 \quad \text{and} \quad F^2 > 4EG, \\[3mm] -\dfrac{G}{F}, & E = 0, \end{cases} \tag{62}
$$

for $\hat{q}_{xx} < 0$.

The hole collapse pressure and passive shear failure pressure for the weak plane failure criterion can be, respectively, expressed as

$$
P_L^{(WP)} = \max_{\theta \in [0, 2\pi]}\left(P_l^{(WP)}(\theta)\right), \tag{63}
$$

$$
P_U^{(WP)} = \min_{\theta \in [0, 2\pi]}\left(P_u^{(WP)}(\theta)\right). \tag{64}
$$

If the orientation of weak planes is different from that of the isotropic plane of the medium, one only needs to adjust the rotation matrix of equation (54) accordingly so that the stress tensor is projected onto the plane of weakness appropriately.

2.6. Tensile Fracturing Failure. Mathematically, the tensile failure criterion can be written as

$$
f_{WP} = -\sigma_{\min} - T_0, \{<0: \text{stable}; \geq 0: \text{unstable}\}, \tag{65}
$$

where T_0 is the tensile strength that is taken to be positive.

For general anisotropic materials, the magnitude of tensile strength should depend on the orientation of principal stresses relative to the anisotropy symmetric plane, as the tensile strength normal to the planes is generally different from the one parallel to them. However, the difference between tensile strength at different directions is usually small and difficult to measure, so the isotropic tensile failure criterion is used in the following derivation.

Substitute $\sigma_{\min}$ with σ_2 (equation (15)) in equation (65), the tensile failure criterion becomes

$$
\sqrt{gP_w^2 + hP_w + s} = eP_w + f + T_0. \tag{66}
$$

Note that the solution to the above equation is also constrained by the magnitude of radial stress at the hole wall:

$$
\sigma_3 = P_w > -T_0. \tag{67}
$$

Following the same analysis procedure, the lower and upper bounds for the safe hole pressure can be obtained as

$$P_l^{(TF)}(\theta) = \begin{cases} \max\left(\dfrac{-F - \sqrt{F^2 - 4EG}}{2E}, -T_0\right), & E > 0 \quad \text{and} \quad F^2 > 4EG, \\[3mm] -T_0, & \text{else}, \end{cases}$$

$$P_u^{(TF)}(\theta) = \begin{cases} \dfrac{-F + \sqrt{F^2 - 4EG}}{2E}, & E \neq 0 \quad \text{and} \quad F^2 > 4EG, \\[3mm] -\dfrac{G}{F}, & E = 0, \end{cases}$$

$$(68)$$

with

$$\begin{aligned} E &= g - e^2, \\ F &= h - 2e(f + T_0), \\ G &= s - (f + T_0)^2. \end{aligned} \tag{69}$$

The minimum $P_u^{(TF)}$ throughout the hole wall is the tensile fracture initiation pressure that is given as

$$P_t = \min_{\theta \in [0, 2\pi]} \left(P_u^{(TF)}(\theta)\right). \tag{70}$$

2.7. Summary of the Steps for Hole Stability Analysis

(1) Divide the hole azimuth from 0° to 180° evenly into N intervals. The sampling points in azimuth are denoted as

$$\theta_n = n \cdot \Delta\theta, \quad n = 0, 1, \ldots, N - 1, \tag{71}$$

where $\Delta\theta$ is the scanning interval.

Because the cylindrical hole stress variations are symmetric with respect to the hole axis, the failure evaluation only needs to be performed at azimuths from 0° to 180°.

(2) Based on the given boundary stress conditions and material properties, calculate the coefficients e, f, g, h, and s (equation (17)) at θ_n ($n = 0, 1, \ldots, N-1$). These coefficients are independent of the hole pressure.

(3) Calculate the hole collapse pressure and passive shear failure pressure of the material matrix using equations (38) and (39) for the Mohr–Coulomb model and equations (46) and (47) for the Drucker–Prager model.

(4) Calculate the hole wall collapse pressure and passive shear failure pressure of the weak planes using equations (63) and (64).

(5) The final collapse pressure that accounts for the failure of both medium matrix and weak planes can be obtained as

$$P_c = \max\left(P_L^{(M)}, P_L^{(WP)}\right), \tag{72}$$

where $P_L^{(M)}$ represents the matrix collapse failure pressure that is calculated from equation (38) or (45) for the Mohr–Coulomb model or Drucker–Prager model, respectively.

(6) Similar to step (5), the final passive shear failure pressure can be given as

$$P_s = \min\left(P_U^{(M)}, P_U^{(WP)}\right), \tag{73}$$

where $P_U^{(M)}$ represents the matrix passive shear failure pressure that is calculated from equation (39) or (47) for the two different shear failure models of the matrix.

(7) The fracture initiation pressure is given by equation (70).

3. Conclusions

A complete workflow for cylindrical hole stability analysis in general laminated materials using an analytical approach is presented. Solutions of critical hole pressure for the Mohr–Coulomb model, Drucker–Prager model, weak plane model, and tensile failure model are given. This workflow can be applied to the stability analysis of arbitrary cylindrical hole in general TI media and is also applicable to degenerate isotropic media. In a TI medium, the effect of strength anisotropy is accounted for through constraining the hole collapse pressure by consolidating a shear failure model for the material matrix and the weak plane failure model. Also, it has been shown that it is necessary to consider both the lower and upper bounds of the stable hole pressure region in shear failure analysis, because collapse failure and passive shear failure can occur together at the hole wall.

Appendix

Analytical Solution for Hole Stress Distribution in an Arbitrary TI Medium

An overview of the derivation of the analytical solution for circular hole stress distribution in an arbitrary TI medium is presented here (refer to the paper of Fang [17] for more details). Because the hole stress solution is derived in HCS, the material stiffness matrix and boundary stress tensor need to be first transformed from GCS to HCS before performing the stress calculation. The stiffness matrix in HCS is given as

$$\mathbf{C} = \mathbf{M}^{(1)} \cdot \mathbf{C}' \cdot \mathbf{M}^{(1)T}, \tag{A.1}$$

with

$$\mathbf{C}' = \mathbf{M}^{(2)} \cdot \mathbf{C}^{(g)} \cdot \mathbf{M}^{(2)T}, \tag{A.2}$$

$$\mathbf{M}^{(1)} = \begin{bmatrix} \cos^2\theta_c & \sin^2\theta_c & 0 & 0 & 0 & -\sin 2\theta_c \\ \sin^2\theta_c & \cos^2\theta_c & 0 & 0 & 0 & \sin 2\theta_c \\ 0 & 0 & 1 & 0 & 0 & 0 \\ 0 & 0 & 0 & \cos\theta_c & \sin\theta_c & 0 \\ 0 & 0 & 0 & -\sin\theta_c & \cos\theta_c & 0 \\ \dfrac{1}{2}\sin 2\theta_c & -\dfrac{1}{2}\sin 2\theta_c & 0 & 0 & 0 & \cos 2\theta_c \end{bmatrix}, \tag{A.3}$$

$$\mathbf{M}^{(2)} = \begin{bmatrix} \cos^2\theta_a\cos^2\theta_i & \sin^2\theta_a\cos^2\theta_i & \sin^2\theta_i & -\sin\theta_a\sin(2\theta_i) & -\cos\theta_a\sin(2\theta_i) & \sin(2\theta_a)\cos^2\theta_i \\ \sin^2\theta_a & \cos^2\theta_a & 0 & 0 & 0 & -\sin 2\theta_a \\ \cos^2\theta_a\sin^2\theta_i & \sin^2\theta_a\sin^2\theta_i & \cos^2\theta_i & \sin\theta_a\sin(2\theta_i) & \cos\theta_a\sin(2\theta_i) & \sin(2\theta_a)\sin^2\theta_i \\ -\dfrac{1}{2}\sin 2\theta_a\sin\theta_i & \dfrac{1}{2}\sin 2\theta_a\sin\theta_i & 0 & \cos\theta_a\cos\theta_i & -\sin\theta_a\cos\theta_i & \cos(2\theta_i)\sin\theta_i \\ \dfrac{1}{2}\cos^2\theta_a\sin 2\theta_i & \dfrac{1}{2}\sin^2\theta_a\sin 2\theta_i & -\dfrac{1}{2}\sin 2\theta_i & \sin\theta_a\cos(2\theta_i) & \cos\theta_a\cos(2\theta_i) & \dfrac{1}{2}\sin(2\theta_a)\sin(2\theta_i) \\ \dfrac{1}{2}\sin 2\theta_a\cos\theta_i & \dfrac{1}{2}\sin 2\theta_a\cos\theta_i & 0 & -\cos\theta_a\sin\theta_i & \sin\theta_a\sin\theta_i & \cos(2\theta_a)\cos\theta_i \end{bmatrix}, \tag{A.4}$$

where $\mathbf{C}^{(g)}$ and $\mathbf{C}$ are the stiffness matrixes in GCS and HCS, respectively, $\mathbf{C}'$ is an intermediate stiffness matrix, $\mathbf{M}^{(1)}$ and $\mathbf{M}^{(2)}$ are, respectively, the Bond transformation matrixes, θ_a and θ_i are, respectively, the well azimuth and inclination. The angle θ_c, which is related to the orientation of the isotropic plane of the medium, is defined as

$$\theta_c = \begin{cases} \dfrac{1}{2}\cot^{-1}\left(\dfrac{C'_{23} - C'_{13}}{2C'_{36}}\right), & \text{if } C'_{36} \neq 0, \\[3ex] \dfrac{1}{2}\cot^{-1}\left(\dfrac{C'_{44} - C'_{55}}{2C'_{45}}\right), & \text{if } C'_{36} = 0 \text{ and } C'_{45} \neq 0, \end{cases} \tag{A.5}$$

where C'_{ij} are the components of the intermediate stiffness matrix $\mathbf{C}'$.

After transforming the stiffness matrix from GCS to HCS, the components C_{14}, C_{16}, C_{24}, C_{26}, C_{34}, C_{36}, C_{45}, and C_{56} of the stiffness matrix are eliminated. The boundary stress tensor in HCS can be obtained as

$$\boldsymbol{\sigma}^{(0)} = \mathbf{E} \cdot \boldsymbol{\sigma}^{(g)} \cdot \mathbf{E}^T, \tag{A.6}$$

with

$$\mathbf{E} = \begin{bmatrix} \cos\theta_c & -\sin\theta_c & 0 \\ \sin\theta_c & \cos\theta_c & 0 \\ 0 & 0 & 1 \end{bmatrix} \cdot \begin{bmatrix} \cos\theta_i & 0 & -\sin\theta_i \\ 0 & 1 & 0 \\ \sin\theta_i & 0 & \cos\theta_i \end{bmatrix} \cdot \begin{bmatrix} \cos\theta_a & \sin\theta_a & 0 \\ -\sin\theta_a & \cos\theta_a & 0 \\ 0 & 0 & 1 \end{bmatrix}, \tag{A.7}$$

where $\boldsymbol{\sigma}^{(g)}$ and $\boldsymbol{\sigma}^{(0)}$ are the in situ stress tensors in GCS and HCS, respectively.

After transforming the stiffness matrix and boundary stress tensor to HCS, hereafter, the derivation is performed in HCS. In the absence of body force, the equation of static equilibrium can be written as

$$\begin{cases} \dfrac{\partial\sigma_{xx}}{\partial x} + \dfrac{\partial\sigma_{xy}}{\partial y} = 0, \\[2ex] \dfrac{\partial\sigma_{xy}}{\partial x} + \dfrac{\partial\sigma_{yy}}{\partial y} = 0, \\[2ex] \dfrac{\partial\sigma_{xz}}{\partial x} + \dfrac{\partial\sigma_{yz}}{\partial y} = 0. \end{cases} \tag{A.8}$$

The constitutive relation can be rewritten as

$$
\begin{bmatrix} \varepsilon_{xx} \\ \varepsilon_{yy} \\ \varepsilon_{zz} \\ 2\varepsilon_{yz} \\ 2\varepsilon_{xz} \\ 2\varepsilon_{xy} \end{bmatrix} = \begin{bmatrix} a_{11} & a_{12} & a_{13} & 0 & a_{15} & 0 \\ a_{12} & a_{22} & a_{23} & 0 & a_{25} & 0 \\ a_{13} & a_{23} & a_{33} & 0 & a_{35} & 0 \\ 0 & 0 & 0 & a_{44} & 0 & a_{46} \\ a_{15} & a_{25} & a_{35} & 0 & a_{55} & 0 \\ 0 & 0 & 0 & a_{46} & 0 & a_{66} \end{bmatrix} \cdot \begin{bmatrix} \sigma_{xx} \\ \sigma_{yy} \\ \sigma_{zz} \\ \sigma_{yz} \\ \sigma_{xz} \\ \sigma_{xy} \end{bmatrix}, \quad \text{(A.9)}
$$

where $[a_{ij}]$ is the corresponding compliance matrix of **C**.

Because ε_{zz} is equal to zero under the plain strain assumption, σ_{zz} can be expressed as

$$
\sigma_{zz} = -\frac{\left(a_{13}\sigma_{xx} + a_{23}\sigma_{yy} + a_{35}\sigma_{xz}\right)}{a_{33}}. \quad \text{(A.10)}
$$

The compatibility equations of strains are

$$
\begin{cases} \dfrac{\partial^2 \varepsilon_{xx}}{\partial y^2} + \dfrac{\partial^2 \varepsilon_{yy}}{\partial x^2} = \dfrac{\partial^2 \varepsilon_{xy}}{\partial x \partial y}, \\[3mm] \dfrac{\partial \varepsilon_{xz}}{\partial y} - \dfrac{\partial \varepsilon_{yz}}{\partial x} = 0. \end{cases} \quad \text{(A.11)}
$$

The equations of equilibrium (equation (A.8)) can be satisfied by introducing two stress functions $F(x,y)$ and $\psi(x, y)$ such that [18]

$$
\sigma_{xx} = \frac{\partial^2 F}{\partial y^2},
$$

$$
\sigma_{yy} = \frac{\partial^2 F}{\partial x^2},
$$

$$
\sigma_{xy} = -\frac{\partial^2 F}{\partial x \partial y}, \quad \text{(A.12)}
$$

$$
\sigma_{xz} = \frac{\partial \Psi}{\partial y},
$$

$$
\sigma_{yz} = -\frac{\partial \Psi}{\partial x}.
$$

The strains can be expressed with $F(x, y)$ and $\psi(x, y)$ by substituting equations (A.10) and (A.12) into the constitutive relation (equation (A.9)). These strains can then be substituted into the compatibility equations (equation (A.11)) to give the Beltrami–Michell equations of compatibility as follows:

$$
\begin{cases} L_4 F + L_3 \Psi = 0, \\ L_3 F + L_2 \Psi = 0. \end{cases} \quad \text{(A.13)}
$$

Here, L_2, L_3, and L_4 are the differential operators that are defined as

$$
L_2 = \beta_{44}\frac{\partial^2}{\partial x^2} + \beta_{55}\frac{\partial^2}{\partial y^2},
$$

$$
L_3 = (\beta_{25} + \beta_{46})\frac{\partial^3}{\partial x^2 \partial y} + \beta_{15}\frac{\partial^3}{\partial y^3}, \quad \text{(A.14)}
$$

$$
L_4 = \beta_{22}\frac{\partial^4}{\partial x^4} + (2\beta_{12} + \beta_{66})\frac{\partial^4}{\partial x^2 \partial y^2} + \beta_{11}\frac{\partial^4}{\partial y^4},
$$

where β_{ij} is called the reduced strain coefficients [18] and is defined as

$$
\beta_{ij} = a_{ij} - \frac{a_{i3} \cdot a_{j3}}{a_{33}}, \quad i, j = 1, 2, \dots, 6. \quad \text{(A.15)}
$$

The general solution for equation (A.13) is given by Lekhnitskii [18] as

$$
F = 2\text{Re}\left[F_1(z_1) + F_2(z_2) + F_2(z_2)\right],
$$
$$
\Psi = 2\text{Re}\left[\lambda_1 F_1'(z_1) + \lambda_2 F_2'(z_2) + \lambda_3^{-1} F_3'(z_3)\right], \quad \text{(A.16)}
$$

with

$$
\lambda_1 = -\frac{l_3(\mu_1)}{l_2(\mu_1)},
$$

$$
\lambda_2 = \frac{l_3(\mu_2)}{l_2(\mu_2)},
$$

$$
\lambda_3 = -\frac{l_3(\mu_3)}{l_4(\mu_3)}, \quad \text{(A.17)}
$$

$$
l_2 = \beta_{44} + \beta_{55}\mu^2,
$$

$$
l_3 = (\beta_{25} + \beta_{46})\mu + \beta_{15}\mu^3,
$$

$$
l_4 = \beta_{22} + (2\beta_{12} + \beta_{66})\mu^2 + \beta_{11}\mu^4,
$$

where $F_i(z_i)$ $(i = 1,2,3)$ are the analytic functions of the complex variable $z_i = x + \mu_i y$; l_2, l_3, and l_4 are, respectively, the characteristic equations of the differential operators L_2, L_3, and L_4; Re[∗] means taking the real part of an expression. μ_i $(i = 1,2,3)$ are the roots of the following polynomial equation:

$$
l_2(\mu)l_4(\mu) - l_3^2(\mu) = 0. \quad \text{(A.18)}
$$

The explicit solutions for the roots μ_1, μ_2, and μ_3 are (Fang [19])

$$
\mu_1 = \sqrt{\eta_1 + \eta_2},
$$

$$
\mu_2 = -\text{sign}(\delta)\sqrt{\eta_1 + \text{sign}(\delta) \cdot \eta_2}, \quad \text{(A.19)}
$$

$$
\mu_3 = \sqrt{-2\eta_1 - \frac{b}{a}},
$$

with

$$a = \beta_{11}\beta_{55} - \beta_{15}^2, \tag{A.20}$$

$$b = \beta_{11}\beta_{44} + \beta_{55}\left(2\beta_{12} + \beta_{66}\right) - 2\beta_{15}\left(\beta_{25} + \beta_{46}\right), \tag{A.21}$$

$$c = \beta_{22}\beta_{55} + \beta_{44}\left(2\beta_{12} + \beta_{66}\right) - \left(\beta_{25} + \beta_{46}\right)^2, \tag{A.22}$$

$$d = \beta_{22}\beta_{44}, \tag{A.23}$$

$$\eta_1 = -\frac{b}{3a} - \frac{1}{2}\left[\left(\varrho + \sqrt{\delta}\,\right)^{1/3} + \left(\varrho - \sqrt{\delta}\,\right)^{1/3}\right], \tag{A.24}$$

$$\eta_2 = i\frac{\sqrt{3}}{2}\left[\left(\varrho + \sqrt{\delta}\,\right)^{1/3} - \left(\varrho - \sqrt{\delta}\,\right)^{1/3}\right], \tag{A.25}$$

$$\varrho = \frac{bc}{6a^2} - \frac{d}{2a} - \left(\frac{b}{3a}\right)^3, \tag{A.26}$$

$$\delta = \varrho^2 + \left[\frac{c}{3a} - \left(\frac{b}{3a}\right)^2\right]^3, \tag{A.27}$$

$$\text{sign}\,(\delta) = \begin{cases} 1, & \text{if } \delta \geq 0, \\ -1, & \text{if } \delta < 0. \end{cases} \tag{A.28}$$

Substituting equation (A.16) into (A.12), the stresses can be obtained as

$$\begin{cases} \sigma_{xx} = \sigma_{xx}^0 + 2\text{Re}\left[\mu_1^2\phi_1'(z_1) + \mu_1^2\phi_2'(z_2) + \lambda_3\mu_1^2\phi_3'(z_3)\right], \\[2mm] \sigma_{yy} = \sigma_{yy}^0 + 2\text{Re}\left[\phi_1'(z_1) + \phi_2'(z_2) + \lambda_3\phi_3'(z_3)\right], \\[2mm] \sigma_{yz} = \sigma_{yz}^0 - 2\text{Re}\left[\lambda_1\phi_1'(z_1) + \lambda_2\phi_2'(z_2) + \phi_3'(z_3)\right], \\[2mm] \sigma_{xz} = \sigma_{xz}^0 + 2\text{Re}\left[\lambda_1\mu_1\phi_1'(z_1) + \lambda_2\mu_2\phi_2'(z_2) + \mu_3\phi_3'(z_3)\right], \\[2mm] \sigma_{xy} = \sigma_{xy}^0 - 2\text{Re}\left[\mu_1\phi_1'(z_1) + \mu_2\phi_2'(z_2) + \lambda_3\mu_3\phi_3'(z_3)\right], \\[2mm] \sigma_{zz} = -\dfrac{a_{31}\sigma_{xx} + a_{32}\sigma_{yy} + a_{34}\sigma_{yz} + a_{35}\sigma_{xz} + a_{36}\sigma_{xy}}{a_{33}}, \end{cases} \tag{A.29}$$

where $\phi_1(z_1) = F_1'(z_1)$, $\phi_2(z_2) = F_2'(z_2)$, and $\phi_3(z_3) = \lambda_3^{-1}F_3'(z_3)$.

The expressions for $\phi_1'(z_1)$, $\phi_2'(z_2)$, and $\phi_3'(z_3)$ are obtained from the boundary conditions as

$$\phi_1'(z_1) = \frac{1}{2}\gamma_1\left[\left(\mu_3\lambda_2\lambda_3 - \mu_2\right)\left(\sigma_{yy}^0 - i\sigma_{xy}^0 - P_w\right) + \left(\lambda_2\lambda_3 - 1\right)\right. \\ \left. \cdot\left(\sigma_{xy}^0 - i\sigma_{xx}^0 + iP_w\right) + \lambda_3\left(\mu_3 - \mu_2\right)\left(\sigma_{yz}^0 - i\sigma_{xz}^0\right)\right], \tag{A.30}$$

$$\phi_2'(z_2) = \frac{1}{2}\gamma_2\left[\left(\mu_1 - \mu_3\lambda_1\lambda_3\right)\left(\sigma_{yy}^0 - i\sigma_{xy}^0 - P_w\right) + \left(1 - \lambda_1\lambda_3\right)\right. \\ \left. \cdot\left(\sigma_{xy}^0 - i\sigma_{xx}^0 + iP_w\right) + \lambda_3\left(\mu_1 - \mu_3\right)\left(\sigma_{yz}^0 - i\sigma_{xz}^0\right)\right], \tag{A.31}$$

$$\phi_3'(z_3) = \frac{1}{2}\gamma_3\left[\left(\mu_2\lambda_1 - \mu_1\lambda_2\right)\left(\sigma_{yy}^0 - i\sigma_{xy}^0 - P_w\right) + \left(\lambda_1 - \lambda_2\right)\right. \\ \left. \cdot\left(\sigma_{xy}^0 - i\sigma_{xx}^0 + iP_w\right) + \left(\mu_2 - \mu_1\right)\left(\sigma_{yz}^0 - i\sigma_{xz}^0\right)\right], \tag{A.32}$$

with

$$\gamma_i = -\left(\Delta\xi_i\sqrt{\left(\frac{z_i}{R}\right)^2 - 1 - \mu_i^2}\,\right)^{-1}, \tag{A.33}$$

$$\xi_i = \frac{(z_i/R) + \sqrt{(z_i/R)^2 - 1 - \mu_i^2}}{1 - i\mu_i}, \tag{A.34}$$

$$\Delta = \left(\mu_2 - \mu_1\right) + \lambda_2\lambda_3\left(\mu_1 - \mu_3\right) + \lambda_1\lambda_3\left(\mu_3 - \mu_2\right). \tag{A.35}$$

The final solution for the stress tensor can be written as

$$\sigma = \sigma^{(0)} + \sigma^{(i)} + q \cdot P_w, \tag{A.36}$$

with

$$\sigma^{(0)} = \begin{bmatrix} \sigma_{xx}^{(0)} & \sigma_{xy}^{(0)} & \sigma_{xz}^{(0)} \\ \sigma_{xy}^{(0)} & \sigma_{yy}^{(0)} & \sigma_{yz}^{(0)} \\ \sigma_{xz}^{(0)} & \sigma_{yz}^{(0)} & \sigma_{zz}^{(0)} \end{bmatrix}, \tag{A.37}$$

$$\sigma^{(i)} = \begin{bmatrix} \sigma_{xx}^{(i)} & \sigma_{xy}^{(i)} & \sigma_{xz}^{(i)} \\ \sigma_{xy}^{(i)} & \sigma_{yy}^{(i)} & \sigma_{yz}^{(i)} \\ \sigma_{xz}^{(i)} & \sigma_{yz}^{(i)} & \sigma_{zz}^{(i)} \end{bmatrix}, \tag{A.38}$$

$$q = \begin{bmatrix} q_1 & q_3 & q_4 \\ q_3 & q_2 & q_5 \\ q_4 & q_5 & q_6 \end{bmatrix}, \tag{A.39}$$

where $\sigma^{(0)}$ is the boundary stress tensor, P_w is the hole gas/fluid pressure, and the terms, $\sigma^{(i)}$ and $q \cdot P_w$, are, respectively, the stress alterations induced by the boundary stresses and the hole gas/fluid pressure. The stress components in $\sigma^{(i)}$ are given as

$$\sigma_{xx}^{(i)} = b_1\sigma_{xx}^{(0)} + c_1\sigma_{yy}^{(0)} + d_1\sigma_{xy}^{(0)} + e_1\sigma_{yz}^{(0)} + f_1\sigma_{xz}^{(0)}, \tag{A.40}$$

$$\sigma_{yy}^{(i)} = b_2\sigma_{xx}^{(0)} + c_2\sigma_{yy}^{(0)} + d_2\sigma_{xy}^{(0)} + e_2\sigma_{yz}^{(0)} + f_2\sigma_{xz}^{(0)}, \tag{A.41}$$

$$\sigma_{xy}^{(i)} = b_3\sigma_{xx}^{(0)} + c_3\sigma_{yy}^{(0)} + d_3\sigma_{xy}^{(0)} + e_3\sigma_{yz}^{(0)} + f_3\sigma_{xz}^{(0)}, \tag{A.42}$$

$$\sigma_{xz}^{(i)} = b_4\sigma_{xx}^{(0)} + c_4\sigma_{yy}^{(0)} + d_4\sigma_{xy}^{(0)} + e_4\sigma_{yz}^{(0)} + f_4\sigma_{xz}^{(0)}, \tag{A.43}$$

$$\sigma_{yz}^{(i)} = b_5\sigma_{xx}^{(0)} + c_5\sigma_{yy}^{(0)} + d_5\sigma_{xy}^{(0)} + e_5\sigma_{yz}^{(0)} + f_5\sigma_{xz}^{(0)}, \tag{A.44}$$

$$\sigma_{zz}^{(i)} = -\frac{\left[a_{13}\sigma_{xx}^{(i)} + a_{23}\sigma_{yy}^{(i)} + a_{35}\sigma_{xz}^{(i)}\right]}{a_{33}}. \tag{A.45}$$

The coefficients b_i, c_i, d_i, e_i, f_i ($i = 1, 2, \ldots, 5$), and q_i ($i = 1, 2, \ldots, 6$) in equations (A.39)–(A.45) are expressed by

$$b_1 = -\mathrm{Re}\left[i\gamma_1\mu_1^2\left(\lambda_2\lambda_3 - 1\right) + i\gamma_2\mu_2^2\left(1 - \lambda_1\lambda_3\right) + i\gamma_3\mu_3^2\lambda_3\left(\lambda_1 - \lambda_2\right)\right], \tag{A.46}$$

$$c_1 = -\mathrm{Re}\left[\gamma_1\mu_1^2\left(\mu_2 - \mu_3\lambda_2\lambda_3\right) + \gamma_2\mu_2^2\left(\lambda_1\lambda_3\mu_3 - \mu_1\right) + \gamma_3\mu_3^2\lambda_3\left(\mu_1\lambda_2 - \mu_2\lambda_1\right)\right], \tag{A.47}$$

$$d_1 = \mathrm{Re}\left[\gamma_1\mu_1^2\left(\lambda_2\lambda_3 - 1 + i\mu_2 - i\mu_3\lambda_2\lambda_3\right) + \gamma_2\mu_2^2\left(1 - \lambda_1\lambda_3 + i\mu_3\lambda_1\lambda_3 - i\mu_1\right) + \gamma_3\mu_3^2\lambda_3\left(\lambda_1 - \lambda_2 + i\mu_1\lambda_2 - i\mu_2\lambda_1\right)\right], \tag{A.48}$$

$$e_1 = \mathrm{Re}\left[\gamma_1\mu_1^2\lambda_3\left(\mu_3 - \mu_2\right) + \gamma_2\mu_2^2\lambda_3\left(\mu_1 - \mu_3\right) + \gamma_3\mu_3^2\lambda_3\left(\mu_2 - \mu_1\right)\right], \tag{A.49}$$

$$f_1 = -\mathrm{Re}\left[i\gamma_1\mu_1^2\lambda_3\left(\mu_3 - \mu_2\right) + i\gamma_2\mu_2^2\lambda_3\left(\mu_1 - \mu_3\right) + i\gamma_3\mu_3^2\lambda_3\left(\mu_2 - \mu_1\right)\right], \tag{A.50}$$

$$b_2 = -\mathrm{Re}\left[i\gamma_1\left(\lambda_2\lambda_3 - 1\right) + i\gamma_2\left(1 - \lambda_1\lambda_3\right) + i\gamma_3\lambda_3\left(\lambda_1 - \lambda_2\right)\right], \tag{A.51}$$

$$c_2 = -\mathrm{Re}\left[\gamma_1\left(\mu_2 - \mu_3\lambda_2\lambda_3\right) - \gamma_2\left(\mu_1 - \mu_3\lambda_1\lambda_3\right) + \gamma_3\lambda_3\left(\mu_1\lambda_2 - \mu_2\lambda_1\right)\right], \tag{A.52}$$

$$d_2 = \mathrm{Re}\left[\gamma_1\left(\lambda_2\lambda_3 - 1 + i\mu_2 - i\mu_3\lambda_2\lambda_3\right) + \gamma_2\left(1 - \lambda_1\lambda_3 + i\mu_3\lambda_1\lambda_3 - i\mu_1\right) + \gamma_3\lambda_3\left(\lambda_1 - \lambda_2 + i\mu_1\lambda_2 - i\mu_2\lambda_1\right)\right], \tag{A.53}$$

$$e_2 = \mathrm{Re}\left[\gamma_1\lambda_3\left(\mu_3 - \mu_2\right) + \gamma_2\lambda_3\left(\mu_1 - \mu_3\right) + \gamma_3\lambda_3\left(\mu_2 - \mu_1\right)\right], \tag{A.54}$$

$$f_2 = -\mathrm{Re}\left[i\gamma_1\lambda_3\left(\mu_3 - \mu_2\right) + i\gamma_2\lambda_3\left(\mu_1 - \mu_3\right) + i\gamma_3\lambda_3\left(\mu_2 - \mu_1\right)\right], \tag{A.55}$$

$$b_3 = \mathrm{Re}\left[i\gamma_1\mu_1\left(\lambda_2\lambda_3 - 1\right) + i\gamma_2\mu_2\left(1 - \lambda_1\lambda_3\right) + i\gamma_3\mu_3\lambda_3\left(\lambda_1 - \lambda_2\right)\right], \tag{A.56}$$

$$c_3 = \mathrm{Re}\left[\gamma_1\mu_1\left(\mu_2 - \mu_3\lambda_2\lambda_3\right) - \gamma_2\mu_2\left(\mu_1 - \mu_3\lambda_1\lambda_3\right) + \gamma_3\mu_3\lambda_3\left(\mu_1\lambda_2 - \mu_2\lambda_1\right)\right], \tag{A.57}$$

$$d_3 = -\mathrm{Re}\left[\gamma_1\mu_1\left(\lambda_2\lambda_3 - 1 + i\mu_2 - i\mu_3\lambda_2\lambda_3\right) + \gamma_2\mu_2\left(1 - \lambda_1\lambda_3 + i\mu_3\lambda_1\lambda_3 - i\mu_1\right) + \gamma_3\mu_3\lambda_3\left(\lambda_1 - \lambda_2 + i\mu_1\lambda_2 - i\mu_2\lambda_1\right)\right], \tag{A.58}$$

$$e_3 = -\mathrm{Re}\left[\gamma_1\mu_1\lambda_3\left(\mu_3 - \mu_2\right) + \gamma_2\mu_2\lambda_3\left(\mu_1 - \mu_3\right) + \gamma_3\mu_3\lambda_3\left(\mu_2 - \mu_1\right)\right], \tag{A.59}$$

$$f_3 = \mathrm{Re}\left[i\gamma_1\mu_1\lambda_3\left(\mu_3 - \mu_2\right) + i\gamma_2\mu_2\lambda_3\left(\mu_1 - \mu_3\right) + i\gamma_3\mu_3\lambda_3\left(\mu_2 - \mu_1\right)\right], \tag{A.60}$$

$$b_4 = -\mathrm{Re}\left[i\gamma_1\mu_1\lambda_1\left(\lambda_2\lambda_3 - 1\right) + i\gamma_2\mu_2\lambda_2\left(1 - \lambda_1\lambda_3\right) + i\gamma_3\mu_3\left(\lambda_1 - \lambda_2\right)\right], \tag{A.61}$$

$$c_4 = -\mathrm{Re}\left[\gamma_1\mu_1\lambda_1\left(\mu_2 - \mu_3\lambda_2\lambda_3\right) - \gamma_2\mu_2\lambda_2\left(\mu_1 - \mu_3\lambda_1\lambda_3\right) + \gamma_3\mu_3\left(\mu_1\lambda_2 - \mu_2\lambda_1\right)\right], \tag{A.62}$$

$$d_4 = \mathrm{Re}\left[\gamma_1\mu_1\lambda_1\left(\lambda_2\lambda_3 - 1 + i\mu_2 - i\mu_3\lambda_2\lambda_3\right) + \gamma_2\mu_2\lambda_2\left(1 - \lambda_1\lambda_3 + i\mu_3\lambda_1\lambda_3 - i\mu_1\right) + \gamma_3\mu_3\left(\lambda_1 - \lambda_2 + i\mu_1\lambda_2 - i\mu_2\lambda_1\right)\right], \tag{A.63}$$

$$e_4 = \mathrm{Re}\left[\gamma_1\mu_1\lambda_1\lambda_3\left(\mu_3 - \mu_2\right) + \gamma_2\mu_2\lambda_2\lambda_3\left(\mu_1 - \mu_3\right) + \gamma_3\mu_3\left(\mu_2 - \mu_1\right)\right], \tag{A.64}$$

$$f_4 = -\mathrm{Re}\left[i\gamma_1\mu_1\lambda_1\lambda_3\left(\mu_3 - \mu_2\right) + i\gamma_2\mu_2\lambda_2\lambda_3\left(\mu_1 - \mu_3\right) + i\gamma_3\mu_3\left(\mu_2 - \mu_1\right)\right], \tag{A.65}$$

$$b_5 = \mathrm{Re}\left[i\gamma_1\lambda_1\left(\lambda_2\lambda_3 - 1\right) + i\gamma_2\lambda_2\left(1 - \lambda_1\lambda_3\right) + i\gamma_3\left(\lambda_1 - \lambda_2\right)\right], \tag{A.66}$$

$$c_5 = \text{Re}\left[\gamma_1\lambda_1(\mu_2 - \mu_3\lambda_2\lambda_3) - \gamma_2\lambda_2(\mu_1 - \mu_3\lambda_1\lambda_3) + \gamma_3(\mu_1\lambda_2 - \mu_2\lambda_1)\right], \tag{A.67}$$

$$d_5 = -\text{Re}\left[\gamma_1\lambda_1(\lambda_2\lambda_3 - 1 + i\mu_2 - i\mu_3\lambda_2\lambda_3) + \gamma_2\lambda_2(1 - \lambda_1\lambda_3 + i\mu_3\lambda_1\lambda_3 - i\mu_1) + \gamma_3(\lambda_1 - \lambda_2 + i\mu_1\lambda_2 - i\mu_2\lambda_1)\right], \tag{A.68}$$

$$e_5 = -\text{Re}\left[\gamma_1\lambda_1\lambda_3(\mu_3 - \mu_2) + \gamma_2\lambda_2\lambda_3(\mu_1 - \mu_3) + \gamma_3(\mu_2 - \mu_1)\right], \tag{A.69}$$

$$f_5 = \text{Re}\left[i\gamma_1\lambda_1\lambda_3(\mu_3 - \mu_2) + i\gamma_2\lambda_2\lambda_3(\mu_1 - \mu_3) + i\gamma_3(\mu_2 - \mu_1)\right], \tag{A.70}$$

$$q_1 = \text{Re}\left[\gamma_1\mu_1^2(\mu_2 - \mu_3\lambda_2\lambda_3 + i(\lambda_2\lambda_3 - 1)) + \gamma_2\mu_2^2(\mu_3\lambda_1\lambda_3 - \mu_1 - i(\lambda_1\lambda_3 - 1)) + \lambda_3\gamma_3\mu_3^2(\mu_1\lambda_2 - \mu_2\lambda_1 + i(\lambda_1 - \lambda_2))\right], \tag{A.71}$$

$$q_2 = \text{Re}\left[\gamma_1(\mu_2 - \mu_3\lambda_2\lambda_3 + i(\lambda_2\lambda_3 - 1)) + \gamma_2(\mu_3\lambda_1\lambda_3) - \mu_1 - i(\lambda_1\lambda_3 - 1) + \lambda_3\gamma_3(\mu_1\lambda_2 - \mu_2\lambda_1 + i(\lambda_1 - \lambda_2))\right], \tag{A.72}$$

$$q_3 = -\text{Re}\left[\gamma_1\mu_1(\mu_2 - \mu_3\lambda_2\lambda_3 + i(\lambda_2\lambda_3 - 1)) + \gamma_2\mu_2(\mu_3\lambda_1\lambda_3) - \mu_1 - i(\lambda_1\lambda_3 - 1) + \gamma_3\mu_3\lambda_3(\mu_1\lambda_2 - \mu_2\lambda_1 + i(\lambda_1 - \lambda_2))\right], \tag{A.73}$$

$$q_4 = \text{Re}\left[\gamma_1\mu_1\lambda_1(\mu_2 - \mu_3\lambda_2\lambda_3 + i(\lambda_2\lambda_3 - 1)) + \gamma_2\mu_2\lambda_2(\mu_3\lambda_1\lambda_3) - \mu_1 - i(\lambda_1\lambda_3 - 1)\right] + \gamma_3\mu_3(\mu_1\lambda_2 - \mu_2\lambda_1 + i(\lambda_1 - \lambda_2)), \tag{A.74}$$

$$q_5 = -\text{Re}\left[\gamma_1\lambda_1(\mu_2 - \mu_3\lambda_2\lambda_3 + i(\lambda_2\lambda_3 - 1)) + \gamma_2\lambda_2(\mu_3\lambda_1\lambda_3) - \mu_1 - i(\lambda_1\lambda_3 - 1) + \gamma_3(\mu_1\lambda_2 - \mu_2\lambda_1 + i(\lambda_1 - \lambda_2))\right], \tag{A.75}$$

$$q_6 = -\frac{(a_{31}q_1 + a_{32}q_2 + a_{34}q_5 + a_{35}q_4 + a_{36}q_3)}{a_{33}}. \tag{A.76}$$

Data Availability

Climate and demand data used to support the findings of this study are available from the first author upon request.

Conflicts of Interest

The authors declare that they have no conflicts of interest.

Acknowledgments

References

[1] S. A. Silling, "Reformulation of elasticity theory for discontinuities and long-range forces," *Journal of the Mechanics and Physics of Solids*, vol. 48, no. 1, pp. 175–209, 2000.

[2] S. A. Silling and E. Askari, "A meshfree method based on the peridynamic model of solid mechanics," *Computers & Structures*, vol. 83, no. 17-18, pp. 1526–1535, 2005.

[3] N. Liu, D. Liu, and W. Zhou, "Peridynamic modelling of impact damage in three-point bending beam with offset notch," *Applied Mathematics and Mechanics*, vol. 38, no. 1, pp. 99–110, 2017.

[4] Y. Hu and E. Madenci, "Bond-based peridynamics with an arbitrary poisson's ratio," in *Proceedings of the 57th AIAA/ASCE/AHS/ASC Structures, Structural Dynamics, and Materials Conference*, pp. 1–15, American Institute of Aeronautics and Astronautics, San Diego, CA, USA, 2016.

[5] C. L. Chow, F. Yang, and A. Asundi, "A method of nonlinear damage analysis for anisotropic materials and its application to thin composite laminates," *International Journal of Damage Mechanics*, vol. 1, no. 3, pp. 347–366, 1992.

[6] D. S. Sharma, "Stress concentration around circular/elliptical/triangular cutouts in infinite composite plate," in *Proceedings of the World Congress on Engineering 2011*, vol. 3, pp. 2626–2631, Imperial College, London, UK, 2011.

[7] F. Z. Zaoui, D. Ouinas, and A. Tounsi, "New 2D and quasi-3D shear deformation theories for free vibration of functionally graded plates on elastic foundations," *Composites Part B: Engineering*, vol. 159, pp. 231–247, 2019.

[8] J. L. Mantari, A. S. Oktem, and C. Guedes Soares, "A new higher order shear deformation theory for sandwich and composite laminated plates," *Composites Part B: Engineering*, vol. 43, no. 3, pp. 1489–1499, 2012.

[9] M. H. Santare and J. Lambros, "Use of graded finite elements to model the behavior of nonhomogeneous materials," *Journal of Applied Mechanics*, vol. 67, no. 4, pp. 819–822, 2000.

[10] C. Li, Z. Zou, and Z. Duan, "Multiple isoparametric finite element method for nonhomogeneous media," *Mechanics Research Communications*, vol. 27, no. 2, pp. 137–142, 2000.

[11] J.-H. Kim and G. H. Paulino, "Isoparametric graded finite elements for nonhomogeneous isotropic and orthotropic materials," *Journal of Applied Mechanics*, vol. 69, no. 4, pp. 502–514, 2002.

[12] M. H. Santare, P. Thamburaj, and G. A. Gazonas, "The use of graded finite elements in the study of elastic wave propagation in continuously nonhomogeneous materials," *International Journal of Solids and Structures*, vol. 40, no. 21, pp. 5621–5634, 2003.

[13] C. O. Horgan and A. M. Chan, "The pressurized hollow cylinder or disk problem for functionally graded isotropic linearly elastic materials," *Journal of Elasticity*, vol. 55, no. 1, pp. 43–59, 1999.

[14] J. Ying and H.-M. Wang, "Magnetoelectroelastic fields in rotating multiferroic composite cylindrical structures," *Journal of Zhejiang University—Science A*, vol. 10, no. 3, pp. 319–326, 2009.

[15] J. F. Durodola and O. Attia, "Deformation and stresses in functionally graded rotating disks," *Composites Science and Technology*, vol. 60, no. 7, pp. 987–995, 2000.

[16] Z. Zhu, Y. Li, X. Zhu, and L. Zhu, "A capacity study of composite sandwich cylindrical shell under hydrostatic pressure, part II: calculation," in *Proceedings of the 21st International Conference on Composite Materials*, p. 2292, Chinese Society for Composite Materials, Xi'an, China, 2017.

[17] X. D. Fang, "A stable explicit workflow for borehole stress calculation in tilted transversely isotropic formations," in *Proceedings of the American Rock Mechanics Association Annual Meeting*, Seattle, WA, USA, 2018.

[18] S. G. Lekhnitskii, P. Fern, and J. J. Brandstatter, *Theory of Elasticity of an Anisotropic Elastic Body*, Holden Day, San Francisco, CA, USA, 1963.

[19] X. D. Fang, "A revisit to the Lekhnitskii-Amadei solution for borehole stress calculation in tilted transversely isotropic media," *International Journal of Rock Mechanics and Mining Sciences*, vol. 104, pp. 113–118, 2018.